IEEE Photonics Journal
An IEEE Photonics Society Publication

Open Access

Soliton and Four-Wave Mixing Effects Induced by the Third-Order Dispersion in a Photonic Crystal Fiber With Femtosecond Pulses Pumping at Normal-Dispersion Regime

Volume 7, Number 5, October 2015

Jianshe Li
Shuguang Li
Yuanyuan Zhao
Hui Li
Guiyao Zhou
Hailiang Chen, Student Member, IEEE
Xiaoming Han
Qiang Liu
Ying Han
Zhenkai Fan
Wan Zhang
Guowen An

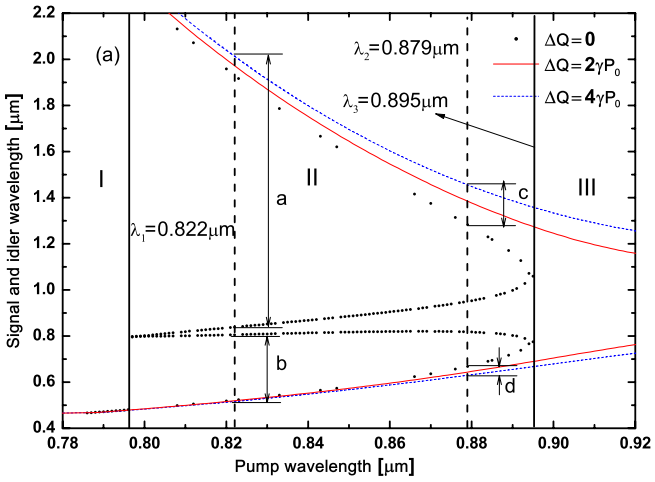

DOI: 10.1109/JPHOT.2015.2468673
1943-0655

Soliton and Four-Wave Mixing Effects Induced by the Third-Order Dispersion in a Photonic Crystal Fiber With Femtosecond Pulses Pumping at Normal-Dispersion Regime

Jianshe Li,[1] Shuguang Li,[1] Yuanyuan Zhao,[1] Hui Li,[1] Guiyao Zhou,[2] Hailiang Chen,[1] *Student Member, IEEE*, Xiaoming Han,[1] Qiang Liu,[1] Ying Han,[3] Zhenkai Fan,[1] Wan Zhang,[1] and Guowen An[1]

[1]State Key Laboratory of Metastable Materials Science and Technology, College of Science, Yanshan University, Qinhuangdao 066004, China
[2]Laboratory of Nanophotonic Functional Materials and Devices, South China Normal University, Guangzhou 510006, China
[3]Key Laboratory for Special Fiber and Fiber Sensor of Hebei Province, College of Information Science and Engineering, Yanshan University, Qinhuangdao 066004, China

DOI: 10.1109/JPHOT.2015.2468673

Manuscript received July 16, 2015; revised August 7, 2015; accepted August 11, 2015. Date of publication August 14, 2015; date of current version August 26, 2015. This work was supported in part by the National Natural Science Foundation of China under Grant 61178026 and Grant 61475134 and in part by the Natural Science Foundation of Hebei Province, China, under Grant E2012203035.
Corresponding author: S. Li (e-mail: shuguangli@ysu.edu.cn).

Abstract: With the homemade solid-core silica-based photonic crystal fiber (PCF), we observe the generation of soliton and four-wave mixing (FWM) when the femtosecond pulse is pumped at 0.822 μm, belonging to the normal-dispersion regime. It is generally acknowledged that FWM is unrelated to third-order dispersion, whereas we use the fourth-order Runge–Kutta method to simulate the PCF properties by taking into account the third-order dispersion or not; the result we got is different from the conventional one. The numerical simulations are greatly consistent with the experiment results, and the FWM is dominated by negative fourth-order and negative sixth-order dispersion in the experiment. The main dynamic process is explained as the soliton, and the FWM generation can be induced by third-order dispersion. We indicate that low Raman threshold has played a very active role in this process, and we propose a conception of stimulated FWM effect in this paper.

Index Terms: Photonic crystal fiber (PCF), four-wave mixing (FWM), pulse propagation, solitons.

1. Introduction

The birth of the photonic crystal fiber (PCF) [1], [2] has opened a new chapter in nonlinear and fiber optics research. The design of the zero dispersion wavelength, selection of the pump wavelength, changes to the pumping position, and the different angles of the laser coupling all have significant impact on the production of the output spectrum. This mainly occurs because the output spectrum is the result of the combination of all kinds of dispersion and nonlinear effects in the PCF. Different

effects need to meet different occurrence conditions, for instance, soliton demands in the anomalous dispersion regime and four-wave mixing (FWM) meeting the phase matching condition [3], etc.

In recent years, supercontinuum (SC) generation has been extensively studied in PCF. It is generally recognized that SC generation is a result of pulse compression and soliton fission in the anomalous dispersion regime, while it is mainly caused by self-phase modulation (SPM) and FWM in the normal dispersion regime. Actually, many dispersion and nonlinear effects can't be ignored in the SC process, such as third-order dispersion (TOD) effect, intrapulse Raman scattering (IPRS) [4], soliton self-frequency shift (SSFS) [5]–[8], cross-phase modulation (XPM) [9], modulation instability [10], and dispersive wave (DW) generation [11]. Alexander M. Heidt *et al.* illustrated the Coherent octave spanning SC generation in all-normal dispersion PCF in the visible and near infrared spectral region by SPM and optical wave breaking (OWB) [12]. Zhigang Chen *et al.* demonstrated the robust generation of near-octave continuum spanning 1.5–3 μm wavelength range by the mechanism involves nonlinear soliton compression, Raman self-frequency shift and resonant emission of DWs in PCF pumped by a femtosecond laser at 1.55 μm [13]. In [14], it is indicated that the FWM and the SSFS play pivotal roles in the process of SC generation. The simulation of [4] showed that the TOD effect mainly influences the symmetry and the flatness of spectra in the normal-dispersion regime, if TOD parameter β_3 want to exert influence on the spectral intensity, it must do by virtue of the IPRS effect, at the same time, IPRS can also be effected by β_3.

In this paper, we design and draw a solid-core silica-based PCF with a simple structure. When we use no initially chirped hyperbolic secant pulse from a Ti:sapphire femtosecond pulsed laser to pump the PCF at the wavelength of 0.822 μm with an average power of 0.64 W, the continuum spectrum is generated from 0.55 μm to 0.975 μm in the visible and near-infrared region, and two separate wave peaks are achieved in the long wavelength region. We explain various phenomena in experiments through numerical simulation, and draw the conclusion about the main dynamics process which is the optical soliton and the FWM effect induced by third-order dispersion.

2. Simulations of the PCF Properties

Fig. 1(a) shows the cross-section of the PCF with un-ordered structure used in the experiment. The air holes are basically hexagonally arranged. The air hole radius of r is about 1.1 μm, and the pitch of Λ is about 2.7 μm. Fig. 1(b) illustration is obtained from Fig. 1(a) by using the digital image processing technology. It's used to guarantee the accuracy of the simulation. Finite element method (FEM) has been used to analyse the properties of the PCF with the illustration in the paper. And the mode field diagram and the electric field direction of the fundamental mode are also shown in the illustration.

Fig. 1(b) shows the variation of the mode-propagation constant β of the fundamental mode as a function of wavelength. In the process of simulation, the material dispersion has been considered by the Sellmeier formula. Fig. 1(c) shows the dispersion parameter D and Group-Velocity dispersion (GVD) parameter β_2 of the fundamental mode as a function of wavelength. The zero dispersion wavelength is at 0.895 μm. Fig. 1(d) shows the third-order dispersion parameter β_3 and fourth-order dispersion parameter β_4 calculated for the fundamental mode as a function of wavelength, it is easy to see that the parameter β_3 is greater than zero from 0.5 μm to 2.5 μm, while the parameter β_4 is less than zero from 0.553 μm to 2.427 μm. In addition, at wavelength $\lambda = 0.822$ μm we also calculated and analyzed the effective mode area of the fundamental model A_{eff} and the nonlinear coefficient γ, whose values are 5.1744 μm^2 and 0.03988 $m^{-1}W^{-1}$, respectively.

3. Experimental Results and Analysis

3.1. Experimental Configuration and Output Spectrum

The experimental schematic diagram is depicted in Fig. 2. A mode-locked Ti:sapphire ultrafast laser is selected, whose pulse full width at half maximum (FWHM) is 120 fs, repetition rate is 76 MHz and center wavelength is 0.800 μm. In order to adjust the incident power, we place a

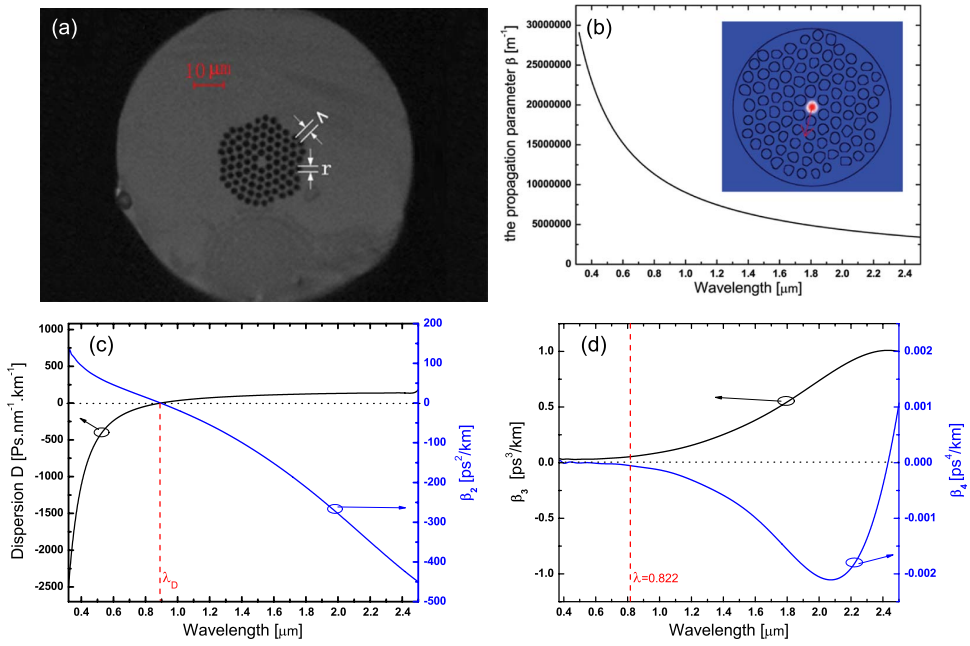

Fig. 1. (a) The cross-section of PCF used in the experiment with parameters $\Lambda = 2.7$ μm and $r = 1.1$ μm. (b) The mode-propagation constant β of the fundamental mode as a function of wavelength. (c) The dispersion parameter D and GVD parameter β_2 calculated for the fundamental mode. The vertical dashed line corresponds to the zero dispersion wavelength of 0.895 μm. (d) The parameter β_3 and β_4 of the fundamental mode as a function of wavelength.

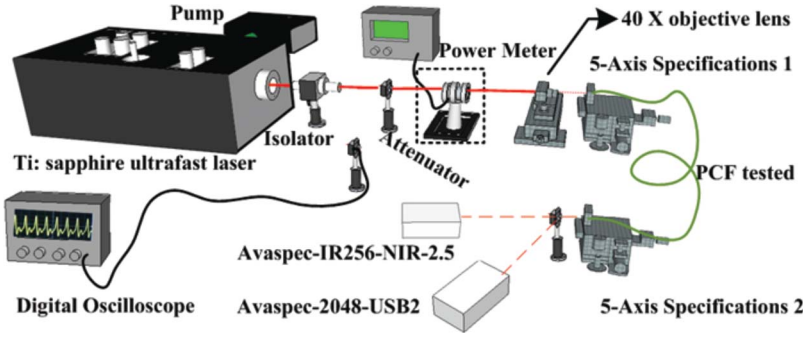

Fig. 2. The experimental schematic diagram.

variable optical attenuator into the light path. The 40 X objective lens is used to couple the input laser light to the core of a 4 m PCF. We specify that P_{in} is the average incident power before the 40 X objective lens (This is the power that measured in the position of Fig. 2 by power meter). Two kinds of optical spectrum analyzers (OSA) of Avaspec-2048-USB2 and Avaspec-IR256-NIR-2.5 are used to measure the spectra at the wavelengths from 0.2 to 1.1 μm and from 0.9 to 2.5 μm in experiment, respectively. Fig. 3 shows the spectrum when the pump wavelength is 0.822 μm and P_{in} are 0.2 W, 0.3 W, 0.4 W, 0.5 W, and 0.64 W, respectively. Fig. 4 shows the spectrum which is obtained by Avaspec-2048-USB2 when the pump transmits 4 m in the PCF and P_{in} is 0.64 W and the pump wavelengths are 0.780 μm, 0.790 μm, 0.800 μm, 0.810 μm, and 0.822 μm, respectively. Although, in order to show weaker peak2, peak3, and peak4, the pump peaks in Fig. 3(a)–(e) look saturated, but the observed spectra in the experiments are not saturated, and the original pump peaks are the standard hyperbolic secant type.

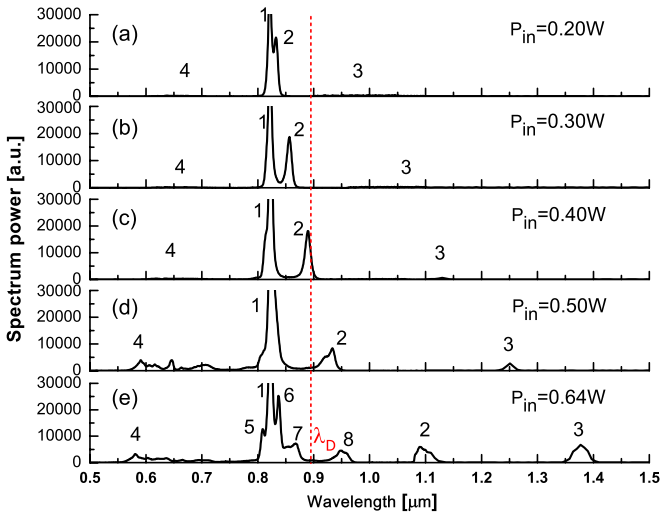

Fig. 3. The experimental output spectrum with the pump laser operating of $\lambda_p = 0.822$ μm and an average input power P_{in} of 0.2 W, 0.3 W, 0.4 W, 0.5 W, and 0.64 W, respectively.

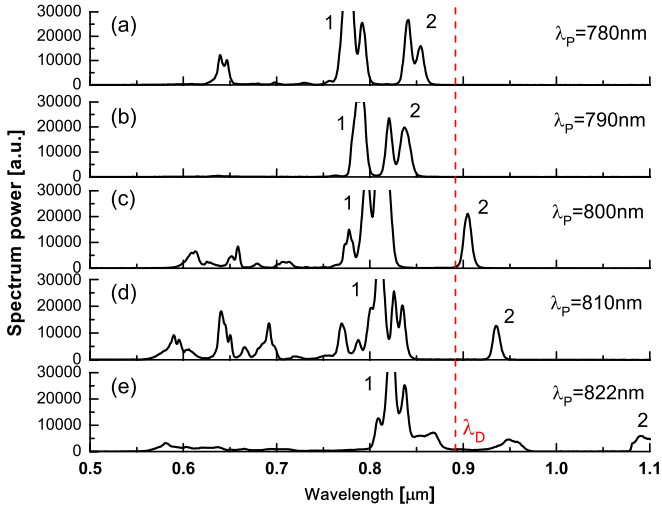

Fig. 4. The experimental output spectrum with an average input power of $P_{in} = 0.64$ W and the pump laser operating wavelengths λ_p of 0.780 μm, 0.790 μm, 0.800 μm, 0.810 μm, and 0.822 μm, respectively.

The spectral components in the shorter wavelength region are simple when peak 2 transmits in the normal-dispersion regimes, as shown in Figs. 3(a)–(c) and 4(a) and (b), while the clear dispersive wavelength bands (DWB) appear on the short wavelength regions when peak 2 transmits in the anomalous-dispersion regimes as shown in Figs. 3(d) and (e), and 4(c)–(e). All these prove DWB generation is related to the wavelength position of peak 2. The following analysis will show that the peak 2 will transform into soliton to get on with transmission when it is located in the anomalous-dispersion regime.

3.2. Simulations of FWM

During the process of FWM, the phase matching condition is [15]–[17]:

$$\triangle\beta + \triangle Q = 0 \tag{1}$$

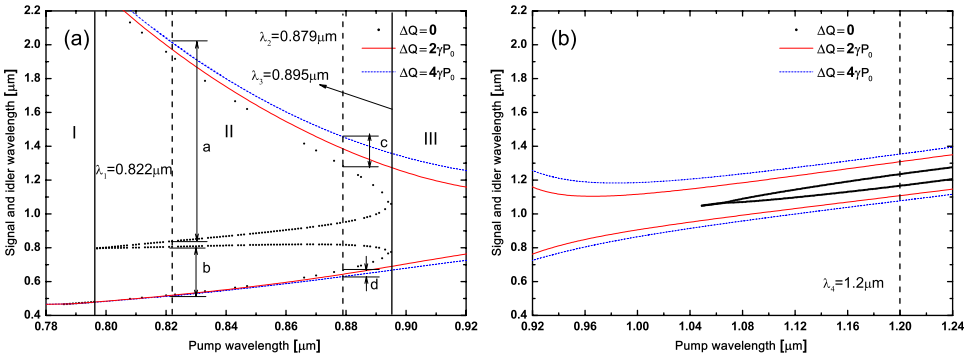

Fig. 5. The phase matching contours with the nonlinear phase mismatch $\triangle Q$ of $4\gamma P_0$, $2\gamma P_0$, and zero, respectively. The incident power is 0.64 W, and the pump wavelength is (a) from 0.78 μm to 0.92 μm and (b) from 0.92 μm to 1.24 μm.

where $\triangle\beta$ is the linear phase mismatch term which can be expressed as $\triangle\beta = \beta_s + \beta_a - 2\beta_p$, where β_s, β_a and β_p are the propagation constants of the signal wave (Stokes wave), the idler wave (anti-Stokes wave), and the pump wave, respectively. $\triangle Q$ is the nonlinear phase mismatch term which is in the region of $0 \leq \triangle Q \leq 4\gamma P_0$, where γ is the nonlinear coefficient, P_0 is the peak power of the pumping. The range of $\triangle Q$ determines the size of the parametric gain generated by the FWM. When $\triangle Q$ is $2\gamma P_0$, the best of phase match and the maximum parametric gains can be obtained. The edge of parametric gain is determined by zero and $4\gamma P_0$.

By using (1), Fig. 5 shows the relationships of the phase matching curves of the PCF with the nonlinear phase mismatch $\triangle Q$ of $4\gamma P_0$, $2\gamma P_0$, and zero, respectively, when the pump wavelength is 0.822 μm and the incident power P_{in} is 0.64 W. In the picture the horizontal axis represents pump wavelength, and the vertical axis represents the signal or the idler wavelength. When the nonlinear phase mismatch is $2\gamma P_0$, it means that the signal and idler waves have maximum gain, and we express the situation with red solid line in Fig. 5. When the nonlinear phase mismatch is $4\gamma P_0$ and zero, it indicates corresponding to minimum gain situation when the FWM effect occurring, we, respectively, express the two situations with blue short dash and black discontinuity point. The points with the same horizontal coordinate value whose vertical coordinates are greater than the horizontal coordinate and also between the range where $\triangle Q = 0$ and $\triangle Q = 4\gamma P_0$ correspond to the signal wave matching points (see Fig. 5). On the contrary, if the vertical coordinates is smaller than horizontal coordinate, these are the idler wave matching points. In order to better show details of the plot, Fig. 5 is divided into (a) and (b): two plans according to the wavelength range.

Simulations show that the corresponding signal wave or the idler wave is discontinuous distributed when the nonlinear phase mismatch is 0 as in Fig. 5(a), which reflects that the size of the gain boundary is greatly affected by the pump wavelength; in this case, when we select a certain pump wavelength, the gain waveband can be very wide or can be very narrow. By using the two black vertical solids in the 0.797 μm and 0.895 μm in the figure, the whole pump wavelength ranges are divided into three regions of I, II, and III. In region I, the signal and the idle wave bands which are surrounded by $\triangle Q = 0$ and $\triangle Q = 4\gamma P_0$ under the same pump wavelength are very narrow. It shows that pumping at any wavelength of region I can meet the phase matching condition for the occurrence of FWM, but the range of the gain band is very small. In region III, because the curve of $\triangle Q = 0$ does not exist, when FWM occurs, the low gain band of the signal wave gets together with the idle wave, it shows that any pump wavelength in this region can meet the phase matching condition for the occurrence of FWM effect, and the generated signal wave and idle wave are getting completely together. It is easy to generate broadband continuous spectrum. In region II, the curve of $\triangle Q = 0$ is not continuous, so when the FWM occurs, the region of the signal wave and the idle wave will greatly depend on the position of the pumping wave. For example, when the pump wavelength is $\lambda_1 = 0.822$ μm, the ranges of the signal and idle wave band are region a $(0.839 \sim 2.013$ μm$)$ and region b

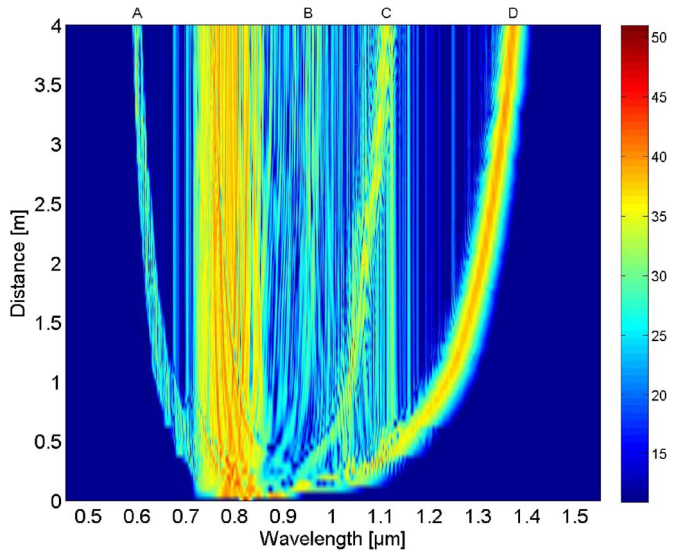

Fig. 6. The relationship of the frequency domain amplitude as transmission distance with the pump wavelength of $\lambda_p = 0.822$ μm and the incident power of $P_{in} = 0.64$ W.

$(0.806 \sim 0.516$ μm$)$, and their wave band sizes are 1.174 μm and 0.290 μm, respectively, while the pump wavelength is $\lambda_2 = 0.879$ μm; the signal and idle wave band ranges are both relatively small; and the sizes of the wave band are only 0.173 μm and 0.039 μm, respectively, which correspond to the region c $(1.283 \sim 1.456$ μm$)$ and region d $(0.669 \sim 0.630$ μm$)$, respectively, in the figure.

3.3. Transmission Simulations

It is generally thought that when the pulse is pumped at the normal-dispersion regime, it is difficult to generate optical soliton and FWM effect in the transmission, but in our experiments, they are all clearly observed. FWM is usually considered only related to even-order dispersions. However it is proved that FWM generation can be induced by third-order dispersion in specific conditions in this paper. Usually, in the spectral broadening experiments, the broadening of SPM will be first observed, and then, the broadenings of optical soliton and FWM are observed, but in our experiments, it is found that the occurrence of SPM may lag behind that of the soliton and FWM.

In order to explain the experimental phenomena, we use the fourth-order Runge–Kutta method [18] to solve the generalized nonlinear Schrodinger equation (GNLSE) in [19], and the frequency-domain and time-domain graphs are plotted with the hyperbolic secant pulse operating wavelengths λ_p of 0.822 μm and an average input power of $P_{in} = 0.64$ W, as shown in Figs. 6–8; the loss is not taken into account in the simulation. The 15th-order dispersion is considered in Fig. 6 (i.e., taking into account all the order dispersions below 15th-order). Fig. 6 shows the four wave peaks of A, B, C, and D have been produced, when the transmission distance is only 0.1 m, these several peaks move further away from the pump wavelength with the increase of transmission distance.

Fig. 7 shows (a) the experimental and (b) simulated output spectrum with the pulse transmission of 4 m in the PCF. Fig. 7(a) is the enlargement of Fig. 3(e), which corresponds to the case of transmission distance of 4 m in Fig. 6. It is observed that the positions of the wave peaks are virtually identical between Fig. 7(a) and (b) and that the experiment research and theory simulation have a very good consistency. Fig. 8 shows the time-domain graphs which take into account different dispersion orders with the transmission distance of 4 m. The third-order and even-order dispersion values used in the simulation are listed in Table 1. When considering only the second-order dispersion, as shown in Fig. 8(a), the time-domain amplitude

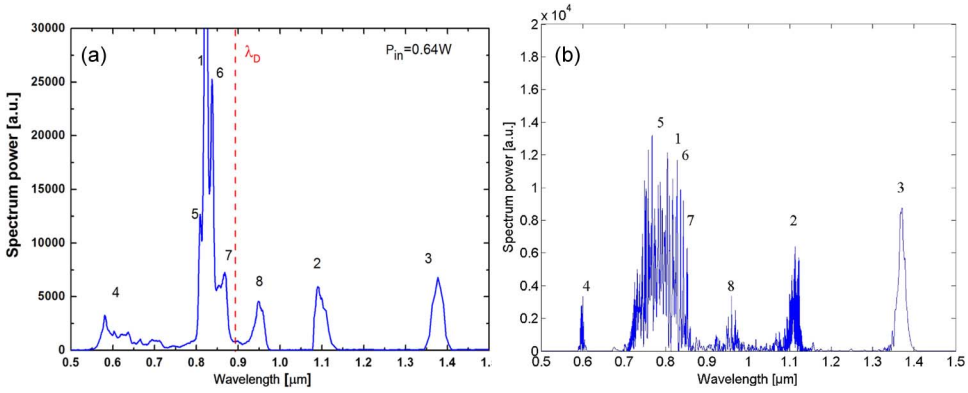

Fig. 7. (a) Experimental and (b) simulated output spectrum with an average input power of $P_{in} =$ 0.64 W and the pump laser operating wavelength of $\lambda_p = 0.822$ μm.

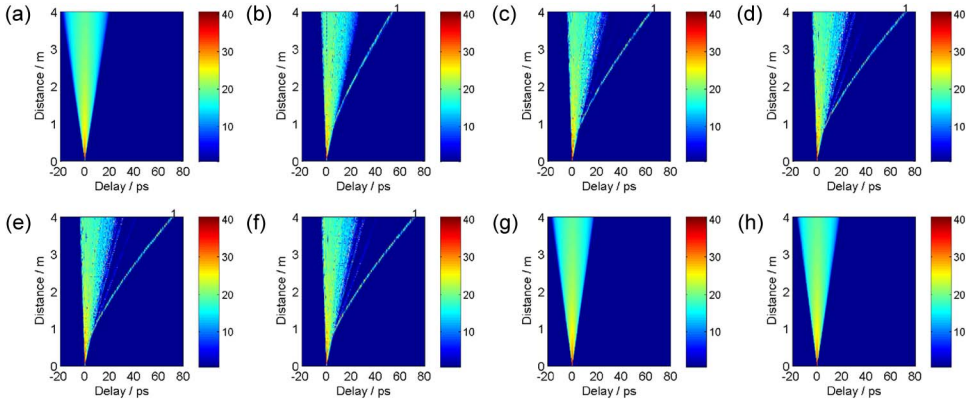

Fig. 8. The time domain amplitudes are changed by transmission distances when we consider the (a) second, (b) third, (c) fourth, (d) sixth, (e) eighth, (f) 14th, (g) fourth expect of third, and (h) 14th expect of third-order dispersion in simulations, respectively.

symmetrically broadens. While considering the third-order dispersion, as shown in Fig. 8(b), the separated peak 1 is quickly established on the trailing edge of the pulse with the increasing of transmission distance and moves nearly to 53.5 ps after transmitting 4 m, the spectral components become much richer than those with just the second-order dispersion is considered. However, if the fourth-order dispersion is considered, peak 1 moves near to 64 ps after transmitting 4 m, as shown in Fig. 8(c). When the sixth-order or higher order dispersion is considered, the location of peak 1 is almost unchanged and stays nearly at 70 ps shown in Fig. 8(d)–(f). While the fourth-order or fourteenth-order except of third-order dispersion is considered in Fig. 8(g) and (h), the pulse has almost the same symmetric spectrum broadening as shown in Fig. 8(a). Through the above analysis, we can see that the spectrum will not asymmetrically broaden when we consider all the other dispersion orders except third-order parameters. This indicates the spectrum asymmetric broadening and peak 1 generation are mainly caused by the third-order dispersion parameter. At the same time, we are also aware of that the degree of the spectral broadening has been accelerated by the fourth and sixth-order dispersions when the third-order dispersion is taken into account, and the impact of higher even-order dispersions can be ignored.

When peak 2 transfers in the normal-dispersion regime, as shown in Fig. 3(a)–(c), the spectrum components of short wavelength region is relatively simple, while P_{in} increases to 0.5 W, the peak 2 begins to transfer into the anomalous-dispersion regime, as shown in Fig. 3(d) and (e), the dispersion wave bands from 0.6 to 0.8 μm belonging to short wavelength region are observed with the energy attenuation of peak 2. The occurrence of dispersion wavelength bands related to

TABLE 1

The third-order and even-order dispersion values of the fundamental mode of the PCF with the pump laser operating wavelength λ_p at 0.822 μm

second-order Ps^2/km	third-order Ps^3/km	fourth-order Ps^4/km	sixth-order Ps^6/km
11.210684	0.054448933	-5.6334679 $\times 10^{-5}$	-1.5023817 $\times 10^{-10}$
eighth-order Ps^8/km	**tenth-order Ps^{10}/km**	**twelfth-order Ps^{12}/km**	**fourteenth-order Ps^{14}/km**
-6.2479994 $\times 10^{-15}$	-1.5124790 $\times 10^{-19}$	2.8480841 $\times 10^{-23}$	-2.1110654 $\times 10^{-27}$

the location's moving of the peak 2 from the normal-dispersion regime to the anomalous-dispersion regime is the typical characteristics of soliton and DW transmission. Therefore, peak 2 translates into a soliton when it locates at the anomalous-dispersion regime. The location of peak 2 is changed by increasing the pump wavelength with the incident power of 0.64 W, as shown in Fig. 4. The same conclusion can be obtained.

Fig. 3 shows that peak 3 and peak 4 have been produced when the average incident power is just 0.2 W (note that the two peaks are not obvious in the picture because the power conversion efficiency is very low.), the two peaks always come in pairs, which is consistent with the phenomena of FWM. In Fig. 7(a), peak 3 is around 1.37 μm and peak 4 is around 0.58 μm, which are located in gain bands a and b (shown in Fig. 5), respectively. In this situation, FWM generation is possible in theory, but the two wavelengths are not in the complete phase matching curves of $\triangle Q = 2\gamma P_0$. In [12], it is indicated that it is possible that the FWM process does not exactly meet the phase matching condition in PCF. In order to distinguish the traditional FWM, the FWM is named stimulated FWM (SFWM) which is induced by third-order dispersion in a non-complete phase-matching condition. In [10], [20], and [21], it is indicated that when the pulse is pumped in the normal-dispersion regime of the PCF, modulation instability lead by the negative fourth-order dispersion parameter will occur and play a positive role on the FWM effect generation. Our previous work [22] has also proved this point. Fig. 8 shows that the spectral broadening process can been accelerated by the fourth-order and the sixth-order dispersion because of SFWM which is dominated by the negative fourth-order and the sixth-order dispersion. We believe that peak 3 and 4 in Fig. 7 are signal wave and idler wave, respectively.

Fig. 3 shows that peak 5 and peak 6 begin to symmetrically appear on both sides of the pump peak 1, when P_{in} increases to 0.64 W. It accords with the characteristics of SPM effect. The lowest incident powers required are 0.20 W and 0.50 W for the SFWM generation (see Fig. 3(a)) and soliton (see Fig. 3(d)), respectively. Compared with most experiments, the SPM effect lags behind the SFWM and soliton generation which is obvious in our experiments, it's mainly because that the broadening of SPM is inhibited by the second-order dispersion parameter β_2 in normal-dispersion regime [23]. Fig. 7 shows that a depth oscillation is produced between the peak 7 and peak 8 and its oscillation strength suddenly drops very low. In addition, a distinct subsidence area is also formed in the vicinity of zero-dispersion wavelength, because of the impact of β_2 [24].

Silva *et al.* have found that stimulated Raman scattering can increase the efficiency of the FWM for a certain frequency detuning [25]. In [26], it is shown that when pump power exceeds the Raman threshold, the rapid transfer of power from the pump wavelength to the longer wavelength region will occur, and it will quickly produce spectral redshift. The Raman threshold is calculated by the approximate equation [26]

$$P_0^{cr} \approx \frac{16 A_{eff}}{g_R L_{eff}} \tag{2}$$

where P_0^{cr} is peak power of the Raman threshold; A_{eff} is the effective mode area; g_R is the Raman gain coefficient; $g_R \approx 1 \times 10^{-13}/\lambda_p$, where λ_p is the pumping wave (the unit is μm); L_{eff}

is the effective length of the fiber; $L_{eff} = [1 - exp(-\alpha_p L)]/\alpha_p$, where α_p is the attenuation coefficient of the fiber; and L is the actual length of the fiber.

According to the simulation, when the pump wavelength is 0.822 μm, the effective mode area of the fundamental mode is about 5.2 μm^2, which is only one tenth of the typical value. The threshold which is calculated by (2) influencing the Raman Effect to occur is about 31 mW, while the actual peak power of the pump is about 4×10^5 times that of the former value. It is because of the very low Raman threshold that, the obvious stimulated Raman scattering (SRS) effect occurred, then the efficient SFWM is observed in a non-complete phase matching condition in the experiment. All of these have played an important role in the quick generation of peak 2 shown in Fig. 3 and spectrogram smoothness in the short wavelength region in Fig. 3(e).

As shown in [27], SSFS can be promoted by IPRS, so the low Raman threshold can also affect the SSFS process by IPRS. In Figs. 3(d), (e), 4(c)–(e) and 7, considering the low Raman threshold, peak 2 can keep a lot of energy when transferring from the normal-dispersion regime to the anomalous-dispersion regime by increasing pump power or pump wavelength, and transforms into optical soliton to continue transmitting under the joint action of dispersion and nonlinear effects. Then the optical soliton launches the dispersion wave generation into short wavelength region by Cherenkov radiation effect. Numerical simulation in [28] showed that the Raman-induced spectral shift (RIFS), having its origin in the phenomenon of IPRS occurring inside silica fibers, occurs both in the normal and anomalous-dispersion regimes, whose magnitude is related to pulsewidth. The mechanism of production of peak 2 in Fig. 3 can be explained as the RIFS effect, which is affected by pulse broading. As shown in Fig. 3(a)–(c), the reason why peak 2 can be obviously observed in the normal-dispersion regime is that the process of the pulse broadening is largely promoted by SFWM in the experiments. The theory simulation of [28] is demonstrated perfectly in our experiments.

Through simulation and analysis, the cause of unusual phenomenal occurrence in the experiments can be explained by the following: Since β_3 is greater than 0 at 0.822 μm, the distortion of the pulse shape caused by the TOD effect will result in the tremendous shock in pulse back edge [24], which will cause asymmetric spectrum broadening produced in the long-wavelength and short-wavelength regions [29]. Because of the very low Raman threshold, with the help of the Raman Effect, the SFWM and soliton can be induced to generate by the third-order dispersion; they accelerate spectral broadening further, and at the same time, the broadening process is accompanied with the nonlinear effects of Cherenkov radiation and SPM as well; all of these effects ultimately produce the observed experimental spectrum.

4. The Simulation of Spectrum With the Pump Operating at Zero Dispersion Wavelength and at Anomalous-Dispersion Regime

We also simulated the spectrum with the pump operating at zero dispersion wavelength and at anomalous-dispersion regime, as shown in Fig. 9, to better explain the occurrence of the FWM with the pump operating at normal-dispersion regime. Fig. 9(a) shows that the energy is easily transferred by the way of the soliton and dispersion wave with the pump operating at 0.895 μm. The peaks 1, 2, and 3 are solitons, the peaks 5 and 6 are DWs, and the peak 4 is the signal wave while the FWM generate. From that, we can see that the power conversion efficiency is very high with pump operating at zero dispersion wavelength and the pump power is almost completely converted. Fig. 9(b) shows that the characteristics of soliton-dispersion wave are more obvious with the pump operating at 1.2 μm belonging to the anomalous-dispersion regime. Because of the instability of the parent soliton, the soliton split quickly. The fundamental soliton 4 which has higher energy quickly spread around 1.923 μm, and then soliton 3 and 2, which have lower energy also, respectively, spread to 1.666 μm and 1.419 μm, but the transfer of the energy is not complete, and the energy around the pump wavelength is still very large. Why is there a peak 4 signal wave instead of a soliton? There are two reasons: 1) The peak power of soliton fission is calculated by the equation $P_k = ((2N + 1 - 2k)^2/N^2)P_0$, where N is the order of the soliton; and k is the ordinal of the fundamental soliton, which comes from the fission of

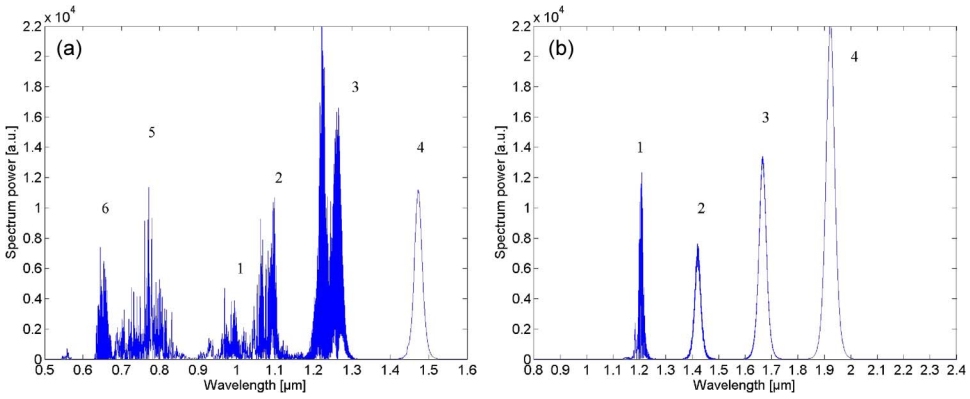

Fig. 9. Simulated output spectrum with the pump laser operating wavelength of (a) $\lambda_p = 0.895$ μm and (b) $\lambda_p = 1.2$ μm, respectively. Other conditions remain unchanged with Fig. 7.

the higher order soliton k = 1 ∼ N. Obviously, the lower the value of k, the larger the energy. The peaks 1, 2, and 3 in Fig. 9(a) tally with the formation rule of the fundamental soliton, while the peak 4 obviously does not tally with that. 2) According to Fig. 5 the peak 4 locate in the range of signal wave gain bands. In summary, it is suitable that peak 4 is explained as the signal wave.

Fig. 5 also illustrate that the range of the gain band becomes narrow as the pump wavelength increases. When the pump wavelength increases to 1.05 μm, the gain band further narrows. It means that as the pump wavelength increases, the phase matching condition for the occurrence of FWM effect is increasingly difficult to meet, and the band gain effect becomes decreasingly less marked. It can be understood as, when the pump wave is in the normal-dispersion regime and the zero dispersion wavelength, the FWM effect is easy to occur for our fiber, and it has played a very positive role for the transfer of the energy. While, when the pump wave is in the anomalous-dispersion regime, the FWM effect is difficult to occur and the transfer of the energy is accomplished by the soliton-dispersion wave effect. Comparing Fig. 7(b) with Fig. 9, the formation of soliton is difficult because the soliton peaks are formed by many small energy peaks, when the pump wavelength is at 0.822 μm and 0.895 μm. This is due to the fact that the soliton cannot exist in the normal-dispersion regime, and it can form when the energy is transferred to the anomalous-dispersion regime, whereas the soliton is easy to form when the pump wavelength is at 1.2 μm. It can be a mark of our fiber to distinguish between soliton and signal wave.

5. Conclusion

In summary, we simulate the pulse transmission process by using the fourth-order Runge–Kutta method to solve generalized nonlinear Schrodinger equation in this paper. The process is analyzed from the aspects of the time domain and frequency domain, and the numerical simulations are in excellent agreement with the experiment results. Through the simulation, many unusual phenomena observed in the experiments are well explained. We discover that the SFWM is dominated by negative fourth-order and negative sixth-order dispersion which satisfy the noncomplete phase matching and can be induced and then produced by third-order dispersion with pumping in the normal-dispersion regime in PCF. To the best of our knowledge, the phenomenon is reported for the first time. Comparing the spectrum simulation of pump at normal-dispersion regime, at zero dispersion wavelength, and at anomalous-dispersion regime, we prove that the FWM occurs in the experiment.

The PCF used in our paper provides a good model to produce a smooth continuous spectrum in the visible light range and study the TOD effect in the normal-dispersion regime. Also, it is of great significance to study the parameter process, the frequency transfer, and fiber lasers. Meanwhile, the structure of the PCF is simple and easy to fabricate.

Acknowledgment

The authors would like to thank the anonymous reviewers for their valuable comments that improved the work presented in this paper.

References

[1] J. C. Knight, T. A. Birks, P. St. J. Russell, and D. M. Atkin, "All-silica single-mode optical fiber with photonic crystal cladding," *Opt. Lett.*, vol. 21, no. 19, pp. 1547–1549, Oct. 1996.
[2] T. A. Birks, J. C. Knight, and P. St. J. Russell, "Endlessly single-mode photonic crystal fiber," *Opt. Lett.*, vol. 22, no. 13, pp. 961–963, Jul. 1997.
[3] J. H. Yuan *et al.*, "Highly efficient wavelength-tunable anti-stokes signal conversion of femtosecond pulses in the fundamental mode of photonic crystal fiber," *IEEE J. Quantum Electron.*, vol. 46, no. 5, pp. 728–733, May 2010.
[4] H. F. Ma, X. Zhang, Q. Jing, Y. Q. Huang, and X. M. Ren, "Effect of intrapulse Raman scattering on broadband amplitude noise of supercontinuum generated in fiber normal dispersion region," *Appl. Opt.*, vol. 51, no. 12, pp. 1962–1967, Apr. 2012.
[5] F. M. Mitschke and L. F. Mollenauer, "Discovery of the soliton self-frequency shift," *Opt. Lett.*, vol. 11, no. 10, pp. 659–661, Oct. 1986.
[6] A. Bendahmane, O. Vanvincq, A. Mussot, and A. Kudlinski, "Control of the soliton self-frequency shift dynamics using topographic optical fibers," *Opt. Lett.*, vol. 38, no. 17, pp. 3390–3393, Sep. 2013.
[7] L. Liu *et al.*, "Soliton self-frequency shift controlled by a weak seed laser in tellurite photonic crystal fibers," *Opt. Lett.*, vol. 38, no. 15, pp. 2851–2854, Aug. 2013.
[8] A. Btourn *et al.*, "Control of supercontinuum generation and soliton self-frequency shift in solid-core photonic band-gap fibers," *Opt. Lett.*, vol. 34, no. 20, pp. 3083–3085, Oct. 2009.
[9] G. Genty, M. Lehtonen, and H. Ludvigsen, "Effect of cross-phase modulation on supercontinuum generated in micro-structured fibers with sub-30 fs pulses," *Opt. Exp.*, vol. 12, no. 19, pp. 4614–4624, Sep. 2004.
[10] M. Droques *et al.*, "Fourth-order dispersion mediated modulation instability in dispersion oscillating fibers," *Opt. Lett.*, vol. 38, no. 17, pp. 3464–3467, Sep. 2013.
[11] N. Akhmediev and M. Karlsson, "Cherenkov radiation emitted by solitons in optical fibers," *Phys. Rev. A, Gen. Phys.*, vol. 51, no. 3, pp. 2602–2607, Mar. 1995.
[12] A. M. Heidt *et al.*, "Coherent octave spanning near-infrared and visible supercontinuum generation in all-normal dispersion photonic crystal fibers," *Opt. Exp.*, vol. 19, no. 4, pp. 3775–3787, Feb. 2011.
[13] Z. G. Chen, A. J. Taylor, and A. Efimov, "Coherent mid-infrared broadband continuum generation in non-uniform ZBLAN fiber taper," *Opt. Exp.*, vol. 17, no. 7, pp. 5852–5860, Mar. 2009.
[14] J. Hu, C. R. Menyuk, L. B. Shaw, J. S. Sanghera, and I. D. Aggarwal, "Supercontinuum generation in an As2Se3-based chalcogenide PCF using four-wave mixing and soliton self-frequency shift," in *Proc. Conf. OFC*, San Diego, CA, USA, Jun. 2009, pp. 1–3.
[15] B. Kuyken *et al.*, "Generation of 3.6 m radiation and telecom-band amplification by four-wave mixing in a silicon waveguide with normal group velocity dispersion," *Opt. Lett.*, vol. 39, no. 6, pp. 1349–1352, Mar. 2014.
[16] L. Zhang *et al.*, "Optical parametric generation with two pairs of gain bands based on a photonic crystal fiber," *Opt. Commun.*, vol. 300, pp. 22–26, Jul. 2013.
[17] M. E. Marhic, K. K. Wong, and L. G. Kazovsky, "Wide-band tuning of the gain spectra of one-pump fiber optical parametric amplifiers," *IEEE J. Sel. Top. Quant. Electron.*, vol. 10, no. 5, pp. 1133–1141, Oct. 2004.
[18] J. Hult, "A fourth-order Runge–Kutta in the interaction picture method for simulating supercontinuum generation in optical fibers," *J. Lightw. Technol.*, vol. 25, no. 12, pp. 3770–3775, Dec. 2007.
[19] J. M. Dudley, "Numerical simulations and coherence properties of supercontinuum generation in photonic crystal and tapered optical fibers," *IEEE J. Sel. Top. Quant. Electron.*, vol. 8, no. 3, pp. 651–659, May/Jun. 2002.
[20] J. D. Harvey *et al.*, "Scalar modulation instability in the normal dispersion regime by use of a photonic crystal fiber," *Opt. Lett.*, vol. 28, no. 22, pp. 2225–2227, Nov. 2003.
[21] S. Pitois and G. Millot, "Experimental observation of a new modulational instability spectral window induced by fourth-order dispersion in a normally dispersive single-mode optical fiber," *Opt. Commun.*, vol. 226, no. 1–6, pp. 415–422, Oct. 2003.
[22] J. S. Li *et al.*, "Experimental research of four-wave mixing and soliton effects in a photonic crystal fiber pumped femtosecond pulses at the wavelength located normal dispersion regime away from the zero dispersion point," *Acta Physica Sinica*, vol. 63, no. 16, Aug. 2014, Art. ID. 164206.
[23] G. P. Agrawal, *Nonlinear Fiber Optics*, 4th ed. San Diego, CA, USA: Academic, Ch. 4, 2006.
[24] G. P. Agrawal, *Nonlinear Fiber Optics*, 4th ed. San Diego, CA, USA: Academic, Ch. 3, 2006.
[25] N. A. Silva, N. J. Muga, and A. N. Pinto, "Influence of the stimulated Raman scattering on the four-wave mixing process in birefringent fibers," *J. Lightw. Technol.*, vol. 27, no. 22, pp. 4979–4988, Nov. 2009.
[26] R. G. Smith, "Optical power handling capacity of low loss optical fibers as determined by stimulated Raman and Brillouin scattering," *Appl. Opt.*, vol. 11, no. 11, pp. 2489–2494, Nov. 1972.
[27] A. C. Judge, S. A. Dekker, R. Pant, C. M. de Sterke, and B. J. Eggleton, "Soliton self-frequency shift performance in As2S3 waveguides," *Opt. Exp.*, vol. 18, no. 14, pp. 14–960–14–968, Jul. 2010.
[28] J. Santhanam and G. P. Agrawal, "Raman-induced spectral shifts in optical fibers: General theory based on the moment method," *Opt. Commun.*, vol. 222, pp. 413–420, Jul. 2003.
[29] F. Leo *et al.*, "Nonlinear symmetry breaking induced by third-order dispersion in optical fiber cavities," *Phys. Rev. Lett.*, vol. 110, Mar. 2013, Art. ID. 104103.